



HAL
open science

Precise Cable-Suspended Pick-and-Place with an Aerial Multi-robot System

A E Jiménez-Cano, Dario Sanalidro, M. Tognon, A. Franchi, J. Cortés

► **To cite this version:**

A E Jiménez-Cano, Dario Sanalidro, M. Tognon, A. Franchi, J. Cortés. Precise Cable-Suspended Pick-and-Place with an Aerial Multi-robot System. *Journal of Intelligent and Robotic Systems*, 2022, 105 (3), pp.68. 10.1007/s10846-022-01668-3 . hal-03748086

HAL Id: hal-03748086

<https://laas.hal.science/hal-03748086>

Submitted on 9 Aug 2022

HAL is a multi-disciplinary open access archive for the deposit and dissemination of scientific research documents, whether they are published or not. The documents may come from teaching and research institutions in France or abroad, or from public or private research centers.

L'archive ouverte pluridisciplinaire **HAL**, est destinée au dépôt et à la diffusion de documents scientifiques de niveau recherche, publiés ou non, émanant des établissements d'enseignement et de recherche français ou étrangers, des laboratoires publics ou privés.

Precise Cable-suspended Pick-and-Place with an Aerial Multi-robot System

A proof of concept for novel robotics-based construction techniques

A.E. Jiménez-Cano · D. Sanalitra · M. Tognon · A. Franchi · J. Cortés

Abstract This work introduces the G-Fly-Crane, a proof-of-concept aerial multi-robot system designed to demonstrate the advantage of using multiple aerial robots as a valuable tool for novel construction techniques, not requiring the use of heavy engines and costly infrastructures. We experimentally demonstrate its capability to perform pick-and-place and manipulation tasks in a construction scenario, with an increased payload capacity and dexterity compared to the single robot case. The system is composed of three aerial robots connected to a platform by three pairs of cables. The platform is equipped with a gripper, enabling the grasping of objects. The paper describes in detail the hardware and software architecture of our prototype and explains the implemented control methods. A shared control strategy incorporates the human operator in the control loop, thus increasing the overall system reliability when performing complex tasks. The paper also discusses the next steps required to bring this technology from indoor laboratory conditions to real-world applications.

This work has been partially funded by the Région Occitanie under contract 2018 003431 - ESR_PREMAT-000160, by the ANR project ANR-17-CE33-0007 ‘MuRoPhen’, and by the European Commission project H2020 AERIAL-CORE (EC 871479)

A.E. Jiménez-Cano¹, D. Sanalitra² and J. Cortés³
LAAS-CNRS, Université de Toulouse, CNRS, 31400 Toulouse, France,
E-mail: ¹antonio-enrique.jimenez-cano@laas.fr
²dario.sanalitra@laas.fr ³juan.cortes@laas.fr

M. Tognon
Autonomous Systems Lab, Department of Mechanical and Process Engineering, ETH Zurich, 8092 Zürich, Switzerland,
E-mail: mtognon@ethz.ch

A. Franchi
Robotics and Mechatronics department, Faculty of Electrical Engineering, Mathematics and Computer Science, University of Twente, 7500 AE Enschede, The Netherlands,
E-mail: a.franchi@utwente.nl

Keywords Aerial Robotics · Multi-robot systems · Shared Control · Novel construction techniques

1 INTRODUCTION

In construction, and more in general in the context of civil engineering, the manipulation of heavy and bulky loads is often required. In some cases, areas difficult to access make the use of ground cranes unfeasible, thus requiring the use of aerial cranes. Large helicopters, for example, are employed to transport and assemble elements for the construction of power transmission lines [27]. Decommissioning of civil structures is also a fundamental and costly task in this field. Both assembly and decommissioning tasks can be accomplished using such heavy aerial machines. However, in addition to being extremely difficult to pilot, they could represent a danger for the construction workers. The use of Unmanned Aerial Vehicles (UAVs) for civil engineering applications, and in particular of multi-rotor platforms, would reduce the above-mentioned risk for the human workers. Moreover, UAVs working autonomously or semi-autonomously could potentially speed up the completion of construction/decommissioning tasks, thus reducing the associated costs. Hence, it is not surprising that the use of aerial robots for construction has gained popularity in the civil engineering domain. In this context, “drone compatible” bricks have recently been designed so that UAVs can rapidly construct real-scale structures, particularly masonry structures, without the use of concrete or other gluing materials [9].

In the field of robotics, researchers have already investigated the problems of transporting objects and assembling small-scale structures. These problems have been firstly addressed by considering a single standard underactuated aerial vehicle equipped with a rigidly-attached gripper (mechanical or magnetic), allowing pick-and-place oper-

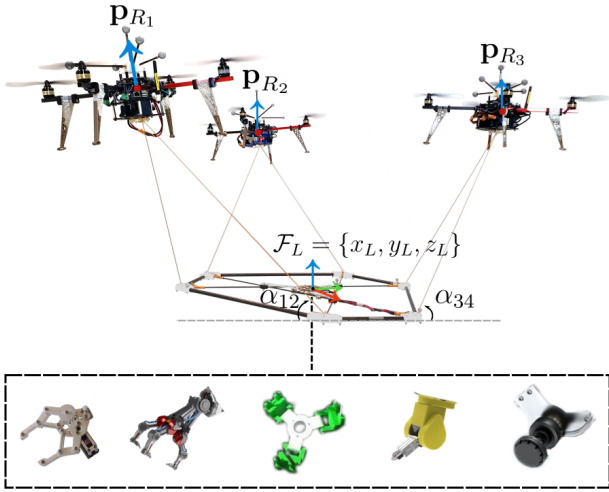


Fig. 1: G-Fly-Crane and its main variables. Several types of grippers can be attached to the platform. In this work, we integrated a simple magnetic gripper.

ations [3, 14, 22]. However, having the load fixed on the aerial robot significantly reduces its agility. Moreover, the coupling of the translational and rotational dynamics makes pick-and-place operations more challenging. A possible solution is to transport the load by means of a cable attached to the robot, which makes it possible to keep the rotational dynamics of the vehicle decoupled from that of translation [6, 24, 26]. Although the simplicity of such a system makes it suitable for transportation purposes, this solution is not optimal for construction uses. The limited payload of a single aerial robot and the inability to control the load attitude make the single-robot single-cable solution unsuitable for pick-and-place and complex manipulation tasks required in construction applications.

To the best of our knowledge, in this work, we introduce for the first time a real cable-suspended aerial multi-robot manipulator able to perform pick-and-place and manipulation operations in a construction/decommissioning scenario. The system developed for this proof of concept, called the *G-Fly-Crane* (Grasping Fly-Crane), is an extension of the *Fly-Crane* [15]. Similarly to the *Fly-Crane*, the *G-Fly-Crane* consists of three quadrotors attached by pairs of cables to a rigid platform. However, the *G-Fly-Crane* is now equipped with a magnetic gripper (see Fig. 1) and incorporates a software architecture to deal with pick-and-place operations involving a shared control approach. The latter represents the main contribution of this work .

This new system is meant to solve the problems previously mentioned: it has an increased payload thanks to the use of multiple quadrotors, and can precisely control all the 6 degrees of freedom (d.o.f.) of the cable-suspended platform, and thus of the grasped object. We shall demon-

strate through experiments, with real pick-and-place and manipulation operations, that these properties make the *G-Fly-Crane* particularly suited for construction and decommissioning applications. This proof of concept represents a preliminary, but fundamental, step in scaling up the system for real-world outdoor applications, with the inclusion of on-board sensors, more sophisticated grippers and larger aerial robots with increased payload capabilities.

Although the *G-Fly-Crane* could control its motion fully autonomously, the complexity of assembly operations in real construction sites, in addition to current safety standards and regulations, requires the possibility for a human operator to supervise and possibly intervene in the control of the system. For this purpose, we designed a shared control strategy, which allows a single user to control both the position and the attitude of the platform, without having to manage the simultaneous control of each robot. Such an assignment would be impossible for a single operator and would require a challenging coordination of multiple operators. Given the operator commands for the platform, the proposed control approach optimally resolves the system redundancy and computes the proper commands for each robot. The proposed control method relies on the kinematic controller presented in [19, 20].

Other multi-robot systems and control strategies have been proposed for the cooperative transportation and manipulation of cable suspended loads. Detailed surveys have been presented in [2, 18]. Different strategies based on inverse dynamics, differential flatness, and formation control, have been proposed to control a team of aerial vehicles connected by cables to a point mass load for transportation purposes [1, 5, 11, 16]. Aiming at more complex manipulation tasks, a two-robot system was considered proposing vision-based [8] and communication-less strategies [25, 28] for the control of a cable-suspended bar. To control the full pose of a cable-suspended rigid load (requiring the ability to attain six-dimensional wrenches) at least three robots connected to three non-collinear points on the load by one cable each are needed [12, 23]. However, to enhance the precision of the system by avoiding internal motions, a *statically rigid* [4] design is preferable. This can be obtained using six (or more) robots connected to six (or more) non-collinear points on the load by one cable each [17]. The *Fly-Crane* [15, 20], and so the *G-Fly-Crane* (as well as similar designs [21]), use a simpler and more efficient statically rigid design involving only three robots, which is the minimum number to fully control the platform pose. This makes it preferable over the other statically-rigid solutions. Nevertheless, the current literature mainly focuses on demonstrating full-pose control capabilities without real interaction tasks. In this work, we go further by experimentally demonstrating the effectiveness of the *G-Fly-Crane* together

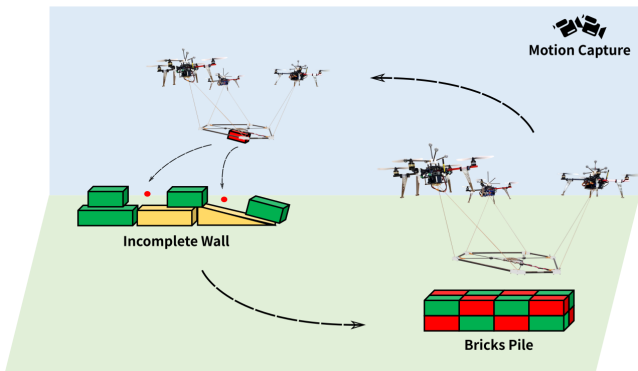


Fig. 2: Scenario designed for the experiments.

with a shared control approach for pick-and-place and manipulation tasks in a construction scenario.

The paper is organized as follows. The G-Fly-Crane hardware and the scenario designed for the experiments are described in Section 2. Section 3 presents the software architecture implemented, and Section 4 describes the proposed control strategy. Experimental results of pick-and-place operations with the G-Fly-Crane are shown in Section 5. Finally, Section 6 concludes the paper with final discussions and comments.

2 EXPERIMENTAL SETUP

Figure 2 shows the scenario designed to demonstrate pick-and-place and manipulation operations with the G-Fly-Crane. This scenario takes place inside an indoor arena equipped with a motion capture system and emulates the construction of a wall. Initially, the wall is incomplete. The two missing bricks, (red bricks in Fig. 2), necessary to complete the wall, are located in a random position on the ground. To increase the task difficulty, the wall was designed simulating an unevenness of the ground, presenting both flat and inclined surfaces. While one brick has to be placed on a flat spot, the other has to be positioned tilted, thus requiring 6D (position and orientation) manipulation capabilities. The bricks weight 0.5 [kg]. Besides, the G-Fly-Crane starts from a random location on the ground.

The G-Fly-Crane is made of three quadrotors (robots) and a platform. Figure 3 shows a graphical scheme of the hardware mounted on each quadrotor. Each robot is equipped with a Mikrokopter FlightCtrl V2.1 and four Mikrokopter ESC's BL-CTRL2.0c using a custom firmware allowing the controller to regulate the propeller speed in closed-loop [7]. An Odroid XU4 is also mounted as on-board PC. The motors are Mikrokopter MK2832 motors with 10x4.5 [inch] propellers. Each quadrotor weights 1.033 [kg] and measures 0.45 [m] diagonally. The available payload of each robot is 0.4 [kg] and, using a battery

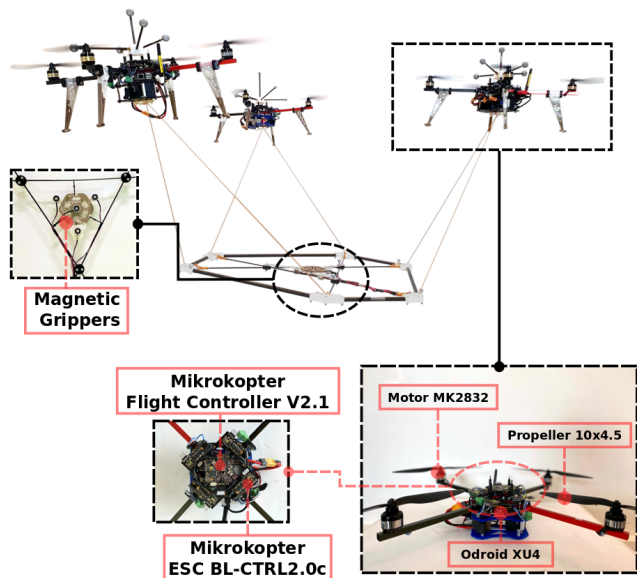


Fig. 3: G-Fly-Crane hardware scheme.

LiPo 4S 2200 mAh, they present 10 minutes of time flight without load.

Six nylon cables are used to attach the robots to the platform, which is made of carbon fiber bars for a total weight of 0.350 [kg]. The platform was designed to dock different types of grippers. For the present work, the G-Fly-Crane is equipped with a gripper consisting of a matrix of four electromagnetic devices. This set-up, chosen after performing several tests, allows compensating undesirable torques while manipulating objects and, adds 0.1 [kg] to the total weight of the platform. The gripper control is implemented on an Arduino Board mounted on one of the robots and connected by USB to its onboard PC. A metal plate glued on top of the bricks allows their manipulation using this magnetic gripper.

Table 1 compares the weight and loading capability of a single quadrotor with respect to (w.r.t.) the one of the G-Fly-Crane system. The comparison is made fair by considering for the G-Fly-Crane system the extra weight introduced by the platform, and that the quadrotors always fly slightly tilted (on average $\chi = 10$ [deg]). This is needed to keep the cables taut and to ensure the balance of forces needed for the 6D manipulation (see [20]). This causes a loss of efficiency of about $1 - \cos(\chi) \simeq 1.5\%$. Following

	Quadrotor weight	Gripper weight	Platform weight	Total weight	Quadrotor payload	Max Load weight
Single quadrotor	1.033	0.1	Not present	1.103	0.4	0.3
G-FlyCrane	1.033×3	0.1	0.35	3.549	0.4×3	0.73

Table 1: Weights and payload capability (in kg) of the G-Fly-Crane compared to a single quadrotor unit.

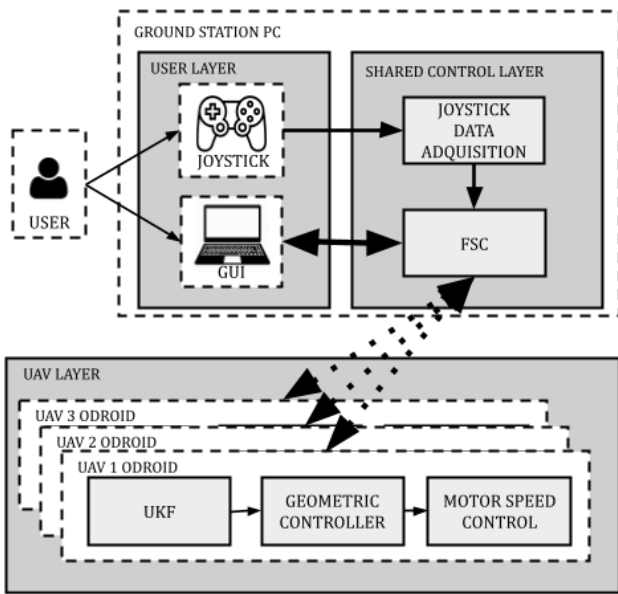


Fig. 4: Software Architecture.

these considerations, the G-Fly-Crane can manipulate loads that are almost 2.5 times heavier compared to what a single quadrotor unit, equipped with an identical gripper, can bear. Furthermore, the G-Fly-Crane has also the capability of manipulating the load in both position and orientation, and of keeping the rotating propellers farther from the environment during the pick-and-place operations. This configuration increases safety, reduces ground effects and creates less downwash on the environment thanks to the larger distance between the propellers and the ground.

3 SOFTWARE ARCHITECTURE

The software architecture for the G-Fly-Crane is implemented using GenoM3, an open-source (BSD-like license) tool developed at LAAS-CNRS to design real-time software architectures. GenoM3 allows the design and production of modules that encapsulate algorithms with inter-process communication, datapool capabilities with external access, and automatic telemetry generation. This framework has been tested in a variety of research robotic prototypes, and used in several European Space Agency (ESA) projects [10].

Figure 4 shows the architecture implemented. It is composed mostly by GenoM modules and divided into three layers, namely: (i) **UAV layer**, which includes the modules related with the flight controllers, state estimation and motor speed controller for each robot; (ii) **shared control layer**, which provides the connection between robots, platform and the user, implementing the controllers needed to operate the whole G-Fly-Crane system; and (iii) **user layer**, the inter-

face with the human operator, which provides the visualization of the system status and the access to safety parameters, controller gains, logs, etc.

The **UAV layer** is composed of standard GenoM3 modules¹ running on the onboard PC of each quadrotor. On the other hand, the **user layer** is composed of a graphical interface and the joystick module running on the ground station PC. Both layers communicate thanks to the **shared control layer**, which runs also on the ground station PC. This layer implements the Fly-Crane Shared Control module (FSC) developed for this application. The FSC is based on the control strategy presented in the next section.

4 CONTROL

The G-Fly-Crane is designed to perform complex tasks related to structure construction. Because of the complexity of the involved problems, such as object localization and classification, obstacle avoidance and so on, real application scenarios and the corresponding regulations require the presence of humans to supervise or operate the robotic systems. However, when a system has a large number of degrees of freedom, such as the G-Fly-Crane, it is impossible to simultaneously command all of them for a single operator. Thus, we have developed the *Fly-Crane Shared Control module* (FSC) to assist the operator. Such a control strategy aims at allowing the operator to focus solely on the end-effector and the proper execution of the task, while the remaining degrees of freedom and the control of each robotic agent are automatically managed.

The control strategy, represented in Fig. 5, implements two flight modes:

- **CRANE**: the modality allows the operator to control the position and orientation of the platform/gripper. It is used during pick-and-place and manipulation operations;
- **MANUAL**: this mode consists of two sub-modes. The first sub-mode maintains the formation shape and lets the human perform a rigid translation of the entire team; the second sub-mode allows the operator to control the position of a single robot while the other two remain stationary. This mode is used during take-off and landing operations and in case of emergency.

Depending on the active flight mode, the FSC module receives and interprets the commands from the human and computes the position and velocity references for the robots, which are sent to the corresponding position controllers.

¹ The full software framework is based on TeleKyb which is open-source and available at <https://git.openrobots.org/projects/telekyb3>

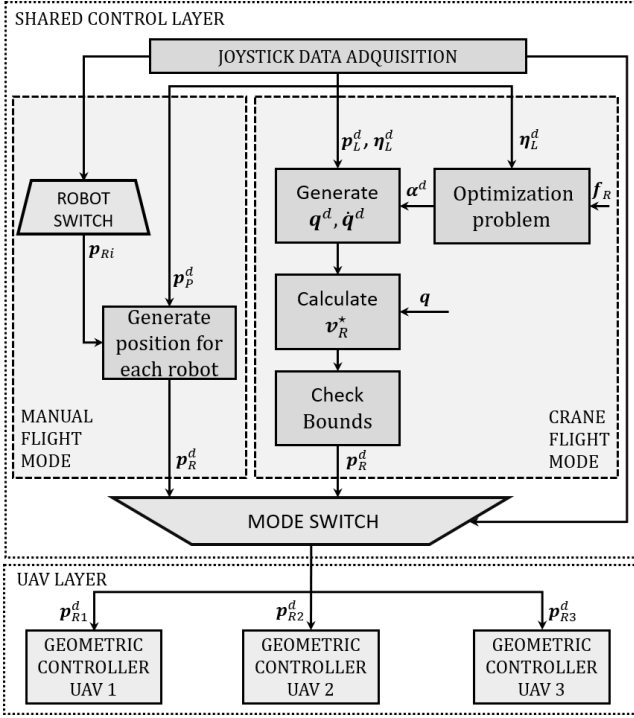


Fig. 5: Control strategy implemented for the G-Fly-Crane.

4.1 Modeling

To present the derivation of the FSC, let us briefly introduce the kinematic model of the G-Fly-Crane (more details are available in [20]). The main variables are schematically represented in Fig. 1. We define two frames:

- an inertial frame $\mathcal{F}_W = \{O_W, \mathbf{x}_W, \mathbf{y}_W, \mathbf{z}_W\}$, where O_W is its origin and $\{\mathbf{x}_W, \mathbf{y}_W, \mathbf{z}_W\}$ are its unit axes;
- a body frame $\mathcal{F}_P = \{O_P, \mathbf{x}_P, \mathbf{y}_P, \mathbf{z}_P\}$ rigidly attached to the platform. \mathcal{F}_P is placed such that O_P coincides with the Center of Mass (CoM) of the platform.

The configuration of the platform is given by $\mathbf{p}_P = [p_{Px} \ p_{Py} \ p_{Pz}]^T \in \mathbb{R}^3$, describing the position of O_P w.r.t. \mathcal{F}_W , and by the Euler angles² $\boldsymbol{\eta}_P = [\phi \ \theta \ \psi]^T \in \mathbb{R}^3$ describing the orientation of \mathcal{F}_P w.r.t. \mathcal{F}_W . The corresponding time derivatives are: its linear velocity $\mathbf{v}_P = [v_{Px} \ v_{Py} \ v_{Pz}]^T = d\mathbf{p}_P/dt \in \mathbb{R}^3$ w.r.t. \mathcal{F}_W , and the Euler angles rates $\dot{\boldsymbol{\eta}}_P = [\dot{\phi} \ \dot{\theta} \ \dot{\psi}]^T \in \mathbb{R}^3$.

The platform is attached by pairs of cables of the same length to three robots whose position w.r.t. \mathcal{F}_W is given by the vectors $\mathbf{p}_{Ri} \in \mathbb{R}^3$ with $i = 1, 2, 3$, respectively. The configuration of each pair of cables w.r.t. \mathcal{F}_P is represented by the angle $\alpha_i \in \mathbb{R}$ between the plane $\{\mathbf{x}_P, \mathbf{y}_P\}$ and the plane shaped by the cables attached to robot i .

² The use of a minimal representation like Euler angles is justified by the fact that the platform will never operate at pitching angles close to $\pi/2$. Therefore any representation singularity problem is not pertinent here.

The system configuration is then entirely described by the variable $\mathbf{q} = [\mathbf{p}_P^T \ \boldsymbol{\eta}_P^T \ \boldsymbol{\alpha}^T]^T \in \mathcal{C} \subset \mathbb{R}^9$, where $\boldsymbol{\alpha} = [\alpha_1 \ \alpha_2 \ \alpha_3]^T \in \mathbb{R}^3$. We also collect the position of all robots in the vector $\mathbf{p}_R = [\mathbf{p}_{R1}^T \ \mathbf{p}_{R2}^T \ \mathbf{p}_{R3}^T]^T$ which can be written as function of \mathbf{q} [20], $\mathbf{p}_R = \mathbf{f}(\mathbf{q})$. Differentiating such a kinematic relation, we obtain the differential kinematic model:

$$\mathbf{v}_R := \dot{\mathbf{p}}_R = \frac{\partial \mathbf{f}(\mathbf{q})}{\partial \mathbf{q}} \dot{\mathbf{q}} = \mathbf{J}(\mathbf{q}) \dot{\mathbf{q}}, \quad (1)$$

where, $\mathbf{v}_R = [v_{R1}^T \ v_{R2}^T \ v_{R3}^T]^T$, and $\dot{\mathbf{q}} = [v_P^T \ \dot{\boldsymbol{\eta}}_P^T \ \dot{\boldsymbol{\alpha}}^T]^T \in \mathbb{R}^9$. The Jacobian matrix $\mathbf{J}(\mathbf{q}) \in \mathbb{R}^{9 \times 9}$ is a square invertible matrix in \mathcal{C} , except for some singular configurations investigated in [21].

4.2 CRANE flight mode

In this mode, the human can directly specify the end-effector pose, i.e., the position and orientation of the platform, \mathbf{p}_P and $\boldsymbol{\eta}_P$, respectively. To do so, we rely on the inverse kinematics controller presented in [20]. Given a desired system trajectory in the configuration space $\mathbf{q}^d(t) = [\mathbf{p}_P^d(t)^T \ \boldsymbol{\eta}_P^d(t)^T \ \boldsymbol{\alpha}^d(t)^T]^T$, the reference velocities of the aerial vehicles are computed as

$$\mathbf{v}_R^* = \mathbf{J}(\mathbf{q}) (\mathbf{K}_q \mathbf{e}_q + \dot{\mathbf{q}}^d), \quad (2)$$

where³ $\mathbf{K}_q = k_q \mathbf{I}_9 \in \mathbb{R}_{>0}^{9 \times 9}$ is a positive definite matrix and $\mathbf{e}_q = \mathbf{q}^d - \mathbf{q}$. In [20], we showed how to optimally compute k_q to guarantee the system stability and the minimum H_∞ gain under parametric uncertainties. We then integrate \mathbf{v}_R^* to obtain the position reference \mathbf{p}_R^* . Both are sent to the geometric position controller [13] running on each aerial vehicle, which implements a PID action based on the position error. We remark that in the considered context, the integral term is sufficient to compensate external disturbances and changes of the platform mass during pick-and-place operations. The desired system trajectory in the configuration space $\mathbf{q}^d(t)$ is defined in a shared way between the human operator and an online local planner. The human specifies the platform position and attitude, while the local planner resolves the redundancy of the system. Thus, we map the joystick commands available to the operator into desired translational and rotational velocities of the platform, i.e., \mathbf{v}_P^d and $\dot{\boldsymbol{\eta}}_P^d$, respectively (see Sec. 4.4). Such quantities are then integrated (starting from the initial configuration) to obtain the desired position and rotation of the platform, i.e., \mathbf{p}_P^d and $\boldsymbol{\eta}_P^d$, respectively. The final quantities to accomplish the desired configuration trajectory, namely $\boldsymbol{\alpha}^d$, are computed through an online local planner [19] as the result of an optimization problem:

$$\boldsymbol{\alpha}^d = \arg \min_{\boldsymbol{\alpha} \text{ s.t. } 0 < \alpha_i < \frac{\pi}{2}} \lambda_1 J_1(\mathbf{q}) - \lambda_2 J_2(\mathbf{q}), \quad (3)$$

³ $\mathbf{I}_n \in \mathbb{R}^{n \times n}$ is the identity matrix of dimension n .

where $J_1(\mathbf{q}), J_2(\mathbf{q})$ are two configuration-dependent cost functions and $\lambda_1, \lambda_2 \in \mathbb{R}_{>0}$ are the corresponding weights. In particular,

$$J_1(\mathbf{q}) = |f_{R1} - f_{R2}| + |f_{R1} - f_{R3}| + |f_{R3} - f_{R2}| \quad (4)$$

$$J_2(\mathbf{q}) = \sqrt{\det(\mathbf{J}(\mathbf{q})\mathbf{J}(\mathbf{q})^\top)}, \quad (5)$$

where $f_{Ri} \in \mathbb{R}_{\geq 0}$ is the thrust intensity delivered by each robot, which depend on the configuration and the known parameters of the system. Solving (3), the local planner computes the cables angles that balance the effort among all the robots ($J_1(\mathbf{q})$) while maximizing the manipulability index⁴ ($J_2(\mathbf{q})$). The time derivative of α^d can be computed numerically or simply assumed zero in the domain of interest. Notice that the distribution of efforts among robots, or in other words the value of $J_1(\mathbf{q})$, also depends on the position of CoM of the platform. In this first proof of concept, we designed the platform and the gripping mechanism such that the position of the platform CoM can be assumed constant during the pick-and-place operations.

4.3 MANUAL flight mode

This flight mode allows the operator to command the position of each aerial vehicle. As for the CRANE flight mode, the operator uses the joystick to send the desired velocities, which are then integrated to obtain the desired position. In this specific flight mode, the operator can choose between two sub-modes:

- MANUAL-1: all robots are moved as a rigid body such that $\mathbf{v}_{R1}^* = \mathbf{v}_{R2}^* = \mathbf{v}_{R3}^* = \mathbf{v}_R^d$,
- MANUAL-2: only one robot is displaced in an independent way while the others maintain their position. In particular $\mathbf{v}_{Ri}^* = \mathbf{v}_R^d$ for a single $i \in \{1, 2, 3\}$, while $\mathbf{v}_{Rj}^* = \mathbf{0}$ for the remaining $j \in \{1, 2, 3\}/\{i\}$.

Notice that $\mathbf{v}_R^d = [v_{Rx}^d \ v_{Ry}^d \ v_{Rz}^d]^\top \in \mathbb{R}^3$ is the velocity command provided by the user.

The MANUAL-1 modality is mostly used for take-off and landing operations while MANUAL-2 in case of emergency. For example, if one the robots face a technical issue, the operator can relocate the others until they reach a safe location, assuming the load and/or the platform can be detached.

4.4 Human interface

The operator interacts with the robotic system through a standard joystick (see Fig. 4). In this section, we describe how the human commands are mapped into directives for

B	v_{Px}^d	v_{Py}^d	$\dot{\phi}^d$	$\dot{\theta}^d$
0	$k_x a_3$	$k_y a_4$	0	0
1	0	0	$k_\phi a_3$	k_θ

Table 2: Commanded horizontal velocity and roll and pitch rates according to the value of B . $k_x, k_y, k_\phi, k_\theta \in \mathbb{R}$ are scaling gains.

the system according to the flight mode. To keep the human interface as similar as possible to the one used by multi-rotor pilots, we employed a similar joystick set up by providing two analogue sticks with two axes each, (a_1, a_2, a_3, a_4) with $a_i \in [-1, 1]$, and several buttons.

CRANE flight mode: In this mode, commands available to the human are mapped into desired linear and rotational velocities of the platform. Mimicking a standard multi-rotor control interface, two axes of one stick are mapped into yaw rate and linear velocity along z_W :

$$\dot{\psi}^d = k_\psi a_1, \quad v_{Pz} = k_z a_2, \quad (6)$$

where $k_\psi, k_z \in \mathbb{R}$ are scaling gains. Through axes a_1 and a_2 , the human operator can control the yaw angle and the altitude of the platform, respectively. To control the planar position and attitude along the remaining x_P and y_P axes, we use the same joystick axes, a_3 and a_4 , according to the status of a button, called $B \in (0, 1)$. The mapping between the axes a_3, a_4 and the desired system commands depending on the value of B are described in Tab. 2.

In practice, with the joystick axes a_3 and a_4 , the operator controls the platform attitude when the button B is pressed, and the platform position otherwise. Separating the control of the horizontal position and the attitude, as well as making the human interface similar to the one used for standard multi-rotors, make the G-Fly-Crane operations simpler and more intuitive.

MANUAL flight mode: In this mode, the mapping is similar to the previous mode, with the difference that the axis a_1 and the B button are ignored. In particular:

$$v_{Rx}^d = k_x a_3, \quad v_{Ry}^d = k_y a_4, \quad v_{Rz}^d = k_z a_2. \quad (7)$$

Additional joystick buttons are used to choose the mode MANUAL-1 or MANUAL-2 and select the robot to be moved.

5 RESULTS

To demonstrate and validate the pick-and-place and manipulation capabilities of the G-Fly-Crane, we present experiments performed in the indoor scenario shown in Section 2.

⁴ Notice that other measures of the manipulability can be used.

A video showing the experiments is provided as supplementary material. In these experiments, the G-Fly-Crane is operated by a single person via a Logitech F310 gamepad, supported by the presented shared control strategy.

In the first experiment, the task is to complete a wall by placing two missing bricks. Figure 6 shows the different phases of the experiment:

1. *Take-off*: the user commands the vertical position of the robots in MANUAL-1 mode to lift the platform;
2. *Pick first brick*: the user commands the position of the platform in CRANE mode ($B = 0$) placing the platform on top of the brick and triggering the magnetic gripper;
- 3-4) *Place first brick*: using the same mode, the user commands the G-Fly-Crane to lift the brick, bring it to the target position, and place it on the incomplete wall;
- 5-8) *Pick and place second brick*: operations 3 and 4 are repeated to pick and place the second brick. However, the second brick has to be placed on the tilted wall. Therefore, when the platform is above the target position and before placing the brick, the operator commands the orientation of the platform ($B = 1$) until the brick is parallel to the wall slope;
- 9-10) *Landing*: finally, the G-Fly-Crane is driven to its initial position for landing.

Considering the more challenging pick-and-place operation of the second brick, Fig. 7 shows the position tracking of the G-Fly-Crane during the phases 5, 6, 7, and 8 starting at time $t_5 = 175$ [s], $t_6 = 195$ [s], $t_7 = 205$ [s], $t_8 = 250$ [s], respectively. The second brick is successfully placed on the wall at time $t = 285$ [s]. Notice that during the pick operation (phase 5), the position error along z_W increases. This is because the user commands a desired platform position such that the magnetic gripper slightly goes inside the brick. Thanks to the natural compliance of the cables, this does not constitute a problem, and the brick can be gently attached once perfectly in contact with the gripping system. During the lift of the brick (phase 6), again, the position error along z_W increases. This is due to the additional mass of the brick that is compensated by the integral action of the robots' position controller only after a few seconds (around $t = 225$ [s]) when the error goes back to zero.

The tracking of the desired trajectory for the attitude and α angles, respectively, are shown in Fig. 8. The noise in these measurements is due to the internal forces acting through the cables and other disturbances generated by communication delays, wind turbulence caused by the rotors of each aerial vehicle, etc. Let us define the position, attitude and cable angles errors as $e_{p_P} = p_P^d - p_P$, $e_{\eta_P} = \eta_P^d - \eta_P$ and $e_\alpha = \alpha^d - \alpha$, respectively. In Tab. 3 we report the mean and variance of the norm of the previous errors.

Figure 8 also shows the extra thrust for each robot, \tilde{f}_{Ri} , defined as the total thrust minus the amount of thrust needed

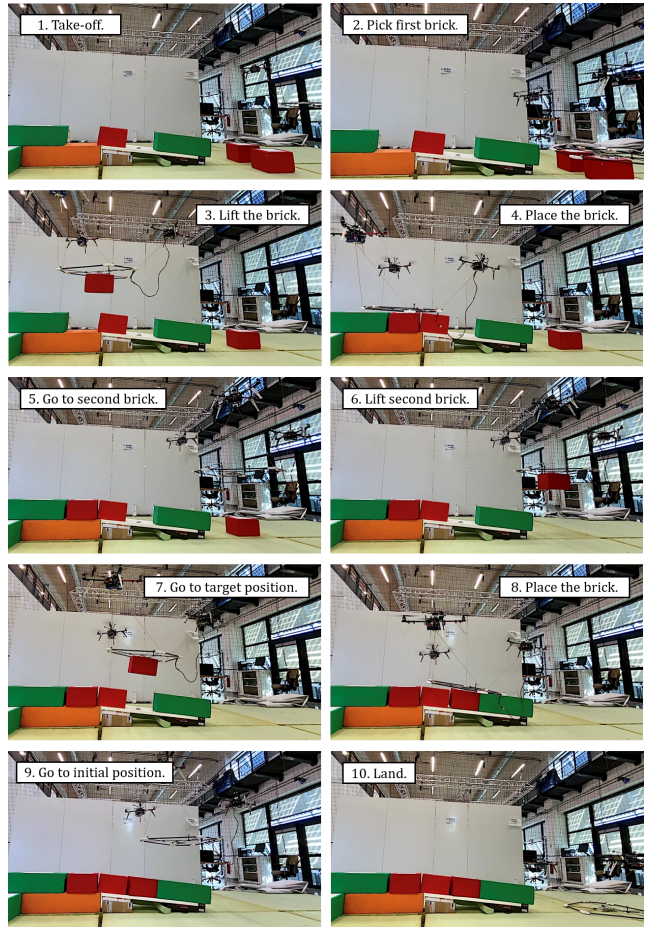


Fig. 6: Snapshots of the wall construction task with the G-Fly-Crane, illustrating different phases.

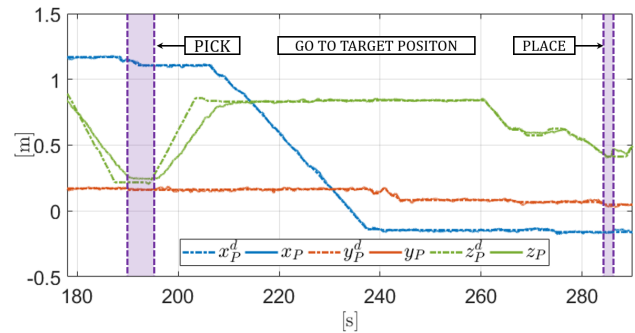


Fig. 7: Position Tracking for the operation of pick-and-place for the second brick.

by each robot to hover the platform without the load. Thanks to the local optimization of the cables angles, α , the thrust values of each robot remain always close to each other indicating a good balance of the effort among the quadrotors. This keeps the energy consumption similar for each of the robots.

At $t = 270$ [s], during phase 8, the brick is located over the wall surface (see video provided as supplementary ma-

	e_{p_P} [m]	e_{η_P} [Deg]	e_{α} [Deg]
Mean	0.026	0.2	0.7
Variance	0.078	1.2	2.8

Table 3: Mean and variance of the norm of the position, attitude and cable angles errors

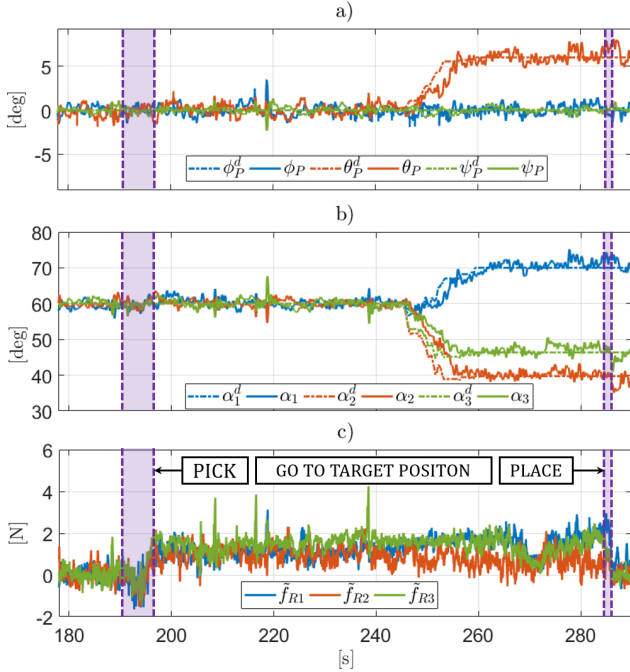


Fig. 8: Tracking of the desired trajectory for the attitude and α angles and comparing with the extra thrust.

terial). Interestingly, as shown in Fig. 8c, the extra thrust for each quadrotor has a sudden decrease because the weight of the brick is temporarily compensated by the contact with the wall.

Additionally, we performed a second experiment further showing the manipulation capabilities of the G-Fly-Crane (see video provided as supplementary material). This test emulates the decommissioning of a structure where bricks must be removed from the inclined wall. As in the previous experiment, the G-Fly-Crane takes off and the operator places it on top of the target brick. Before descending to perform the pick, the pilot provides the commands to adjust the platform orientation according to the inclination of the brick. The brick can be then removed from the wall safely and accurately, thanks to the dexterity provided by the G-Fly-Crane.

6 DISCUSSION AND CONCLUSIONS

For the first time, we have experimentally demonstrated the physical interaction capabilities of an aerial multi-robot

system for complex pick-and-place and manipulation operations in the context of construction scenarios. We have proposed a shared control strategy that allows a single person to operate such a complex robotic system. As a result, the human has complete control over the manipulation operations rather than having to separately provide commands to each quadrotor. The obtained results successfully represent the first proof of concept for the potential use of the G-Fly-Crane in construction. However, we recognize that the presented experimental validation was conducted in an indoor laboratory setting and that there are several challenges ahead in bringing this technology to real-world applications. One of these challenges is the localization of the system (the robots and the platform). In general, a motion capture system (such as the one used in this work) is unsuitable for large outdoor workspaces, and the accuracy provided by a global positioning system is insufficient to perform precise manipulation tasks. A possible solution is the combination of a global positioning system with cameras and other onboard sensors, using VIO algorithms and sensor fusion techniques. Another key consideration is robustness, which is especially significant when dealing with diverse atmospheric conditions or when the system has to interact with the environment. Therefore, in addition to a more robust mechatronic design, robust control approaches will be necessary to enhance the proposed shared control strategy. Moreover, the optimization of the redundancy, i.e., the cables angles, is only local in our current implementation. A global planning method considering internal and external constraints (e.g., obstacles) in addition to an optimal balance of the payload among the robots would be relevant tools to increase robustness and to ease the system's operations. Furthermore, in the future, when new regulations will allow for manipulation activities to be performed with such complex aerial robotic systems, fully autonomous execution of the tasks could be envisioned. For this first proof of concept, we deliberately simplified the grasping problem by considering a magnetic gripper that can easily grasp and release bricks in our demonstration scenario. Nevertheless, the application of the G-Fly-Crane technology to real-world construction tasks will require the integration of more sophisticated automated grasping methods and grippers suited to the shape and material of the manipulated parts. The mentioned improvements are considered as future works.

Acknowledgements The authors would like to thank Quentin Sable from the University of Twente for his contribution to the experimental platform and Anthony Mallet from LAAS-CNRS who collaborated to develop the software architecture.

Fundings

This work has been partially funded by the Région Occitanie under contract 2018 003431 - ESR_PREMAT-000160, by the ANR project ANR-17-CE33-0007 ‘MuRoPhen’, and by the European Commission project H2020 AERIAL-CORE (EC 871479).

Conflict of interest

The authors declare that they have no conflict of interest.

Availability of data and material

Not applicable.

Code availability

Not applicable.

Authors' contributions

A.E.J.C. and D.S.: Original draft preparation, hardware/software development and experimental tests. M.T.: writing - review and editing. A.F. and J.C.: Supervision, funding acquisition, writing - review and editing.

Ethics approval

Not applicable.

Consent to participate

Not applicable.

Consent for publication

Not applicable.

References

1. Bernard, M., Kondak, K., Maza, I., Ollero, A.: Autonomous transportation and deployment with aerial robots for search and rescue missions. *Journal of Field Robotics* **28**(6), 914–931 (2011)
2. Bonyan Khamseh, H., Janabi-Sharifi, F., Abdessameud, A.: Aerial manipulation literature survey. *Robotics and Autonomous Systems* **107**, 221–235 (2018). DOI <https://doi.org/10.1016/j.robot.2018.06.012>
3. Braithwaite, A., Alhinai, T., Haas-Heger, M., McFarlane, E., Kovač, M.: *Tensile Web Construction and Perching with Nano Aerial Vehicles*, pp. 71–88. Springer International Publishing (2018). DOI [10.1007/978-3-319-51532-8_5](https://doi.org/10.1007/978-3-319-51532-8_5)
4. Connelly, R., Guest, S.D.: *Frameworks, tensegrities and symmetry: understanding stable structures*. Cornell University, College of Arts and Sciences (2015)
5. Erskine, J., Chriette, A., Caro, S.: Control and configuration planning of an aerial cable towed system. In: 2019 International Conference on Robotics and Automation (ICRA), pp. 6440–6446. IEEE (2019)
6. Foehn, P., Falanga, D., Kuppaswamy, N., Tedrake, R., Scaramuzza, D.: Fast trajectory optimization for agile quadrotor maneuvers with a cable-suspended payload. *Robotics: science and systems* **13** (2017). DOI [10.15607/RSS.2017.XIII.030](https://doi.org/10.15607/RSS.2017.XIII.030)
7. Franchi, A., Mallet, A.: Adaptive closed-loop speed control of BLDC motors with applications to multi-rotor aerial vehicles. In: 2017 IEEE Int. Conf. on Robotics and Automation, pp. 5203–5208. Singapore (2017)
8. Gassner, M., Cieslewski, T., Scaramuzza, D.: Dynamic collaboration without communication: Vision-based cable-suspended load transport with two quadrotors. In: 2017 IEEE Int. Conf. on Robotics and Automation, pp. 5196–5202. Singapore (2017)
9. Goessens, S., Mueller, C., Latteur, P.: Feasibility study for drone-based masonry construction of real-scale structures. *Automation in Construction* **94**, 458–480 (2018)
10. Ingrand, F., Lacroix, S., Lemai-Chenevier, S., Py, F.: Decisional autonomy of planetary rovers. *Journal of Field Robotics* **24**(7), 559–580 (2007)
11. Klausen, K., Meissen, C., Fossen, T.I., Arcak, M., Johansen, T.A.: Cooperative control for multirotors transporting an unknown suspended load under environmental disturbances. *IEEE Transactions on Control Systems Technology* **28**(2), 653–660 (2020). DOI [10.1109/TCST.2018.2876518](https://doi.org/10.1109/TCST.2018.2876518)
12. Lee, T.: Geometric control of quadrotor uavs transporting a cable-suspended rigid body. *IEEE Transactions on Control Systems Technology* **26**(1), 255–264 (2017)
13. Lee, T., Leoky, M., McClamroch, N.H.: Geometric tracking control of a quadrotor UAV on SE(3). In: 49th IEEE Conf. on Decision and Control, pp. 5420–5425. Atlanta, GA (2010)
14. Lindsey, Q., Mellinger, D., Kumar, V.: Construction with quadrotor teams. *Autonomous Robots* **33**(3), 323–336 (2012)
15. Manubens, M., Devaurs, D., Ros, L., Cortés, J.: Motion planning for 6-D manipulation with aerial towed-cable systems. In: 2013 Robotics: Science and Systems. Berlin, Germany (2013)
16. Marina, H.D., Smeur, E.: Flexible collaborative transportation by a team of rotorcraft. In: 2019 IEEE Int. Conf. on Robotics and Automation, pp. 1074–1080. IEEE (2019)
17. Masone, C., Bühlhoff, H.H., Stegagno, P.: Cooperative transportation of a payload using quadrotors: A reconfigurable cable-driven parallel robot. In: 2016 IEEE/RSJ Int. Conf. on Intelligent Robots and Systems, pp. 1623–1630 (2016)
18. Ollero, A., Tognon, M., Suarez, A., Lee, D.J., Franchi, A.: Past, present, and future of aerial robotic manipulators. *IEEE Transactions on Robotics* **38**(1), 626–645 (2021). DOI [10.1109/TRO.2021.3084395](https://doi.org/10.1109/TRO.2021.3084395)
19. Petitti, A., Sanalidro, D., Tognon, M., Milella, A., Cortés, J., Franchi, A.: Inertial estimation and energy-efficient control of a cable-suspended load with a team of UAVs. In: 2020 Int. Conf. on Unmanned Aircraft Systems. Athens, Greece (2020)
20. Sanalidro, D., Savino, H.J., Tognon, M., Cortés, J., Franchi, A.: Full-pose manipulation control of a cable-suspended load with multiple UAVs under uncertainties. *IEEE Robotics and Automation Letters* **5**(2), 2185–2191 (2020). DOI [10.1109/LRA.2020.2969930](https://doi.org/10.1109/LRA.2020.2969930)
21. Six, D., Briot, S., Chriette, A., Martinet, P.: The kinematics, dynamics and control of a flying parallel robot with three quadrotors. *IEEE Robotics and Automation Letters* **3**(1), 559–566 (2018)

22. Spurný, V., Báča, T., Saska, M., Pěnička, R., Krajník, T., Thomas, J., Thakur, D., Loianno, G., Kumar, V.: Cooperative autonomous search, grasping, and delivering in a treasure hunt scenario by a team of unmanned aerial vehicles. *Journal of Field Robotics* **36**(1), 125–148 (2019)
23. Sreenath, K., Kumar, V.: Dynamics, control and planning for cooperative manipulation of payloads suspended by cables from multiple quadrotor robots. In: *Proceedings of Robotics: Science and Systems*. Berlin, Germany (2013). DOI 10.15607/RSS.2013.IX.011
24. Sreenath, K., Michael, N., Kumar, V.: Trajectory generation and control of a quadrotor with a cable-suspended load-a differentially-flat hybrid system. In: *2013 IEEE International Conference on Robotics and Automation*, pp. 4888–4895. IEEE (2013)
25. Tagliabue, A., Kamel, M., Verling, S., Siegwart, R., Nieto, J.: Collaborative transportation using MAVs via passive force control. In: *2017 IEEE Int. Conf. on Robotics and Automation*, pp. 5766–5773. Singapore (2016)
26. Tang, S., West, V., Kumar, V.: Aggressive flight with suspended payloads using vision-based control. *IEEE Robotics and Automation Letters* **3**(2), 1152–1159 (2018). DOI 10.1109/LRA.2018.2793305
27. Tarapygin, P.P.: Utilization of helicopters in power construction. *Hydrotechnical Construction* **1**(10), 927–933 (1967)
28. Tognon, M., Gabellieri, C., Pallottino, L., Franchi, A.: Aerial co-manipulation with cables: The role of internal force for equilibria, stability, and passivity. *IEEE Robotics and Automation Letters, Special Issue on Aerial Manipulation* **3**(3), 2577 – 2583 (2018). DOI 10.1109/LRA.2018.2803811